Evidence for an active fault below the northwestern Alpine foreland of Switzerland

U. Kastrup, N. Deichmann, A. Fröhlich and D. Giardini

Swiss Seismological Service, Institute of Geophysics, ETH Hönggerberg, CH-8093 *Zürich, Switzerland. E-mail: deichmann@sed.ethz.ch*

SUMMARY

This study is devoted to the analysis of a prominent concentration of earthquakes whose epicenters delineate an active 20–30 km long N–S trending tectonic feature near the town of Fribourg, in the Molasse Basin of western Switzerland. This feature coincides with the possible southward continuation of the NNE–SSW trending Rhine Graben located approximately 80 km further north. In addition these epicenters are located in the vicinity of the Fribourg Syncline and the Alterswil Culmination, whose structural axes are oriented N–S in this area, instead of being aligned with the predominant regional NE–SW structural trend. Most of the earthquakes belong to one of three series of events that occurred over a time span of 2–4 months in 1987, 1995 and 1999. They include four events with magnitudes between 3 and 4 and one with a magnitude of 4.3. Focal depths, constrained by modelling sPMP-PMP traveltime differences with synthetic seismograms, are around 2 km, which places these events in the sedimentary cover. Fault plane solutions correspond to almost pure strike-slip mechanisms with nearly N–S and E–W oriented nodal planes. High-precision relative locations of individual events within the different earthquake clusters as well as of the relative locations of the clusters to each other show that these earthquakes are associated with left lateral motion along a N–S trending fault system. Deep reaching large scale flower structures in the Mesozoic and Tertiary overburden are observed on interpreted seismic profiles, close to the hypocenters. The unusual N–S trend of the Fribourg Syncline can be attributed to movements along these faults during Oligocene and Miocene times. Also magnetic data support the assumption of a N–S striking fault system in the Fribourg area, possibly related to a Permo-Carboniferous trough. Though the direct link between the fault traces in the overburden and the active fault system at depth could not be established in this study, their similar deformational style and their vicinity suggest that they are related. The total length of the inferred fault carries the potential of a magnitude 6 earthquake and thus constitutes a significant source of seismic hazard.

Key words: active faults, earthquakes, seismic hazard, Switzerland.

1 INTRODUCTION

On epicenter maps compiled over the last 25 yr, earthquake clustering can be detected in numerous areas of Switzerland (e.g. Kastrup *et al.* 2004; Deichmann *et al.* 2006). In the Molasse Basin, an area of overall low seismic activity, a zone of increased seismicity is situated south of the Rhine Graben and features several prominent earthquake clusters. Our interest was drawn to a particularly prominent concentration of epicenters near the city of Fribourg in the Molasse Basin of western Switzerland (Figs 1 and 2). The epicenter locations seem to delineate an active N–S trending tectonic feature. This feature coincides with the possible southward continuation of the NNE–SSW trending Rhine Graben located approximately 80 km further north. In addition, these epicenters are located in the vicinity of the Fribourg Syncline and the Alterswil Culmination (Fig. 2), whose structural axes are oriented N–S in this area, instead of being aligned with the predominant regional NE–SW structural trend.

This unusual orientation has already led others to postulate a buried fault in this area (NAGRA 1988).

In this paper we address the relationship of the observed epicenter alignment in the Fribourg area to the regional tectonic setting. To this end we reanalyse the absolute epicentral locations and focal depths of these earthquakes, we determine precise relative locations of individual events within the cluster and derive focal mechanisms for the most prominent events. The results of this seismological analysis are integrated into interpretations of seismic reflection data and geomagnetic surveys to obtain a comprehensive seismotectonic picture of the Fribourg area.

2 TECTONIC SETTING

In the foreland of the Alps the three main tectonic units are the Rhine Graben, the Molasse Basin and the Jura Mountains (Fig. 2).
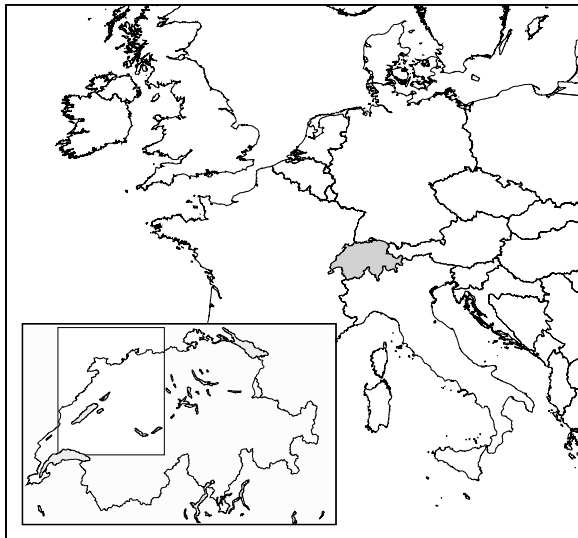
GJI Seismology

Figure 1. Location of study area within Europe and Switzerland. The inner inset corresponds to the area of Fig. 2.

The Rhine Graben is part of a rift system that extends from the western Mediterranean to the North Sea. Its formation north of the Alpine orogenic belt dates back to the most active phase of deformation in the Alps from Eocene to Oligocene times (about 39 Ma) (Illies 1974). Subsidence started in the area of what later became the southern Rhine Graben. During the following Oligocene rifting stage, NNE–SSW striking faults formed; many Rhine Graben faults, however, rejuvenated older Hercynian zones of weakness which had already been reactivated once during Permian times and cut into the basement. The main rifting phase ended in the Miocene (20–15 Ma ago) due to a change in the stress directions, which was probably related to the counterclockwise rotation of the Adriatic plate. While extension was perpendicular to the Rhine Graben faults during the early stages of deformation, the direction of minimum horizontal stress was now oblique to it (NE–SW), (e.g. Ahorner *et al.* 1972; Plenefisch & Bonjer 1997; Kastrup *et al.* 2004). This caused a graben, more favourably oriented to the new stress field, to open up in the area of the present lower Rhine embayment, while the Rhine Graben remained active as a left lateral stike-slip zone. Today seismic activity in the area of the Rhine Graben is consistent with such a deformation. The Molasse Basin covers the area south of the
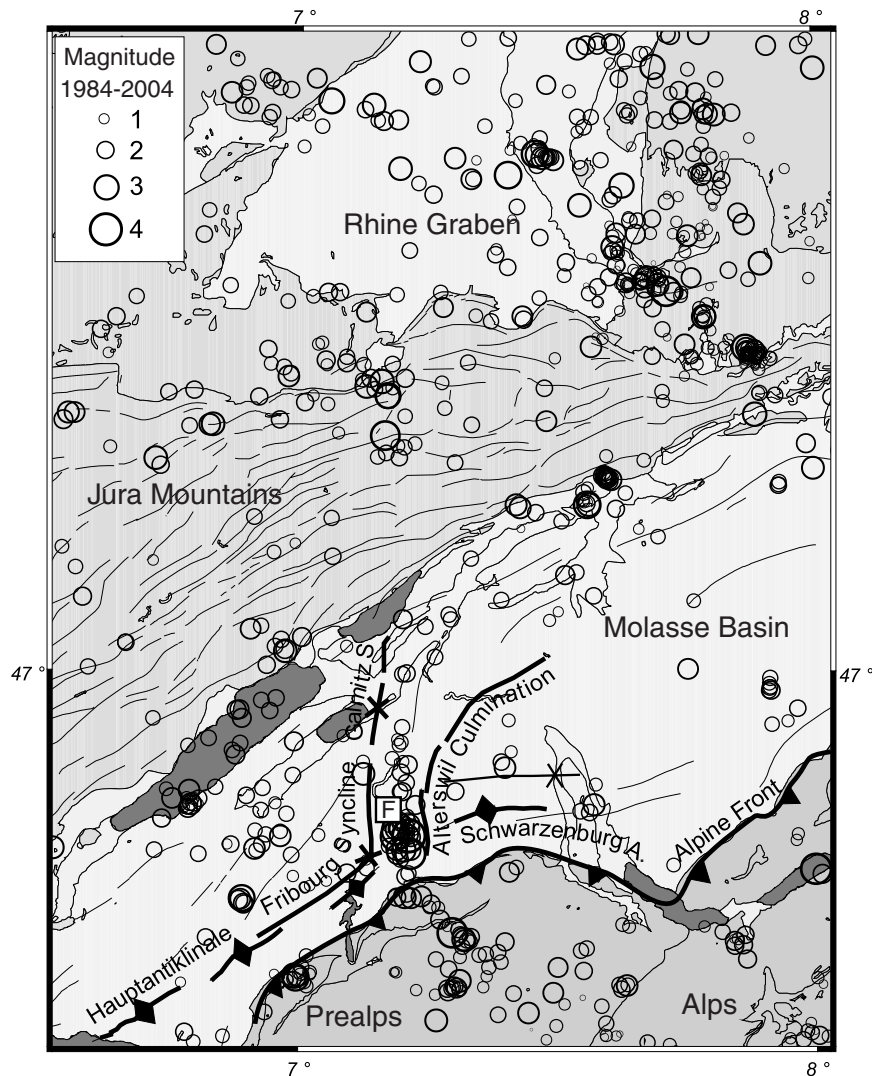

Figure 2. Topographic map of the area studied. Faults are plotted for the whole area, anticlines and synclines only for the larger Fribourg region. Note the bend of the Fribourg Syncline from NW to N and the strike of the Alterswil Culmination, oblique to the general trend of the foldaxes (after Kopp 1946). F denotes the town of Fribourg.

Rhine Graben between the Alps and the Jura Mountains, extending from Lake of Constance to the South of Lake Geneva. It represents the former detrital foreland basin of the Alps during Tertiary times. Oligocene and Miocene clastics were deposited more or less conformably, but with a progressive onlap towards the North on top of the Mesozoic sediments. The thickness of the Molasse succession varies from several hundred meters in the North to 4 km and more in the South (Burkhard 1990). In the area studied, the thickness is about 1 km. Tectonically the Molasse can be divided into three distinct units: the predominantly horizontally bedded Plateau Molasse, the folded Molasse and the steeply dipping thrusted Subalpine Molasse. The area studied here is entirely located in the mildly folded part of the Plateau Molasse, which has been influenced by the late Alpine compressional deformation starting during the upper Middle to Late Miocene (i.e. Laubscher 1985). In the Plateau Molasse the fold axes generally strike NE–SW, approximately parallel to the Jura Belt and the Alpine front (Fig. 2). However, the Fribourg Syncline and the Alterswil Culmination deviate from this general trend (Kopp 1946; Plancherel 1996), (Fig. 2). The Alterswil Culmination east of Fribourg is a classic example of a crossfold. It strikes almost perpendicular to the dominant orientation of the Plateau Molasse structure, the 'Hauptantiklinale', and forms a separating element between the latter and Schwarzenburg Anticline to the east, which trend both parallel to the Alpine front (Kopp 1946). The Fribourg Syncline, which to the southwest of Fribourg follows the general NE–SW strike-direction of the Molasse folds, bends north just south of Fribourg and eventually merges into the Galmiz Syncline (Fig. 2). Interestingly, this transversal zone lies in the southern continuation of the Rhine Graben (Pavoni 1977). However, it is difficult to establish a direct connection between the N–S trending structures and the Rhine Graben, as no large-scale and hardly any small-scale surface faults or fractures are observed in the Molasse sediments. This is different in the Prealps to the South and the adjacent Jura Mountain Belt to the North. In the Jura Mountains, which were formed as a fold and thrust belt around 3–5 Ma ago when Mesozoic sediments where detached along Triassic evaporites, reactivated N–S striking faults have strongly influenced the style of deformation, which is still expressed by bended fold axis and large tear faults.

3 SEISMOLOGICAL INVESTIGATIONS

3.1 Absolute epicenter locations

The seismological part of this study is devoted primarily to a detailed analysis of the prominent N–S alignment of epicenters near the town of Fribourg (Fig. 2). In Fig. 3 we show the epicenters of all the earthquakes located in a 20x50 km region around Fribourg, from November 1983, the date after which digital records are available, until the end of 2004. The 30 earthquakes of particular interest in this study, enclosed by the rectangle in Fig. 3, belong to one of three sequences of events that occurred over a time span of two to four months in 1987, 1995 and 1999. Four of these events have local magnitudes (M_L) between 3 and 4 and one reached M_L 4.3. The seismograms with date, time and magnitudes of all events associated with the three sequences, recorded at station BRI, are shown in Fig. 4. Station BRI is situated almost exactly due East of the epicenters, and the seismograms are aligned on the P-wave arrivals observed at station ROM, which is situated due West (see Fig. 6). Station ROM was chosen as reference, because P-wave arrivals at station BRI could not be identified unequivocally for all events. The
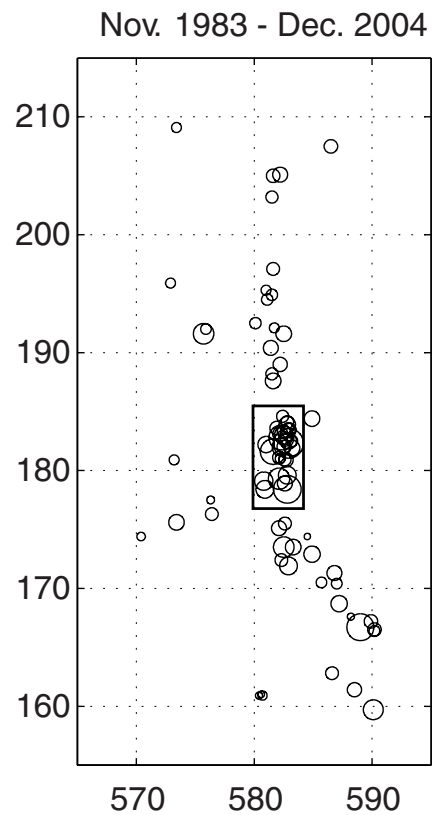

Figure 3. Routinely determined epicenters of all digitally recorded earthquakes in the area of Fribourg, between November 1983 and December 2004. Magnitudes range between M_L 0.9 and 4.3. The rectangle encloses the Fribourg cluster. Axes are labeled in Swiss Cartesian coordinates (km).

relatively consistent alignment of the S-wave arrivals for all events observed at station BRI clearly shows that at least in an EW direction the epicenters must be closely spaced to each other. Moreover, the overall signal similarity, in particular between the events of 1995 and 1999, suggests that the epicenters must be relatively closely spaced even in a NS direction and that focal depths are probably similar as well. The difference in frequency content of the coda waves between the events of 1987 and the later ones visible in Fig. 4 is not seen at other stations, so that it is possible that this difference is due to a change in instrument characteristics.

In the past, source locations were calculated routinely with program HYPO-71 (Lee & Lahr 1972) or with a gridsearch algorithm using a 1-D velocity-depth model that consists of three horizontal layers over a mantle half-space. In this model, the lower-crustal layer is of variable thickness, to account for the large differences in Moho-depth between foreland and Alpine stations. The model also allows for some variations in near-surface geology and in station elevations by using different velocities in the uppermost layer for stations in the Alps and Alpine foreland and by calculating elevation-dependent station delays (see Deichmann *et al.* 2004, for more details). The absolute locations of the Fribourg events given in Fröhlich (1989), Kastrup (2002) and Deichmann *et al.* (2000) were based on these results.

More recently, we have implemented the software package Non-LinLoc (Lomax *et al.* 2000). This procedure is based on a combination of probabilistic earthquake location and non-linear, global search algorithms using nested grids or the Oct-Tree Importance sampling algorithm (Lomax & Curtis 2001). The probabilistic,
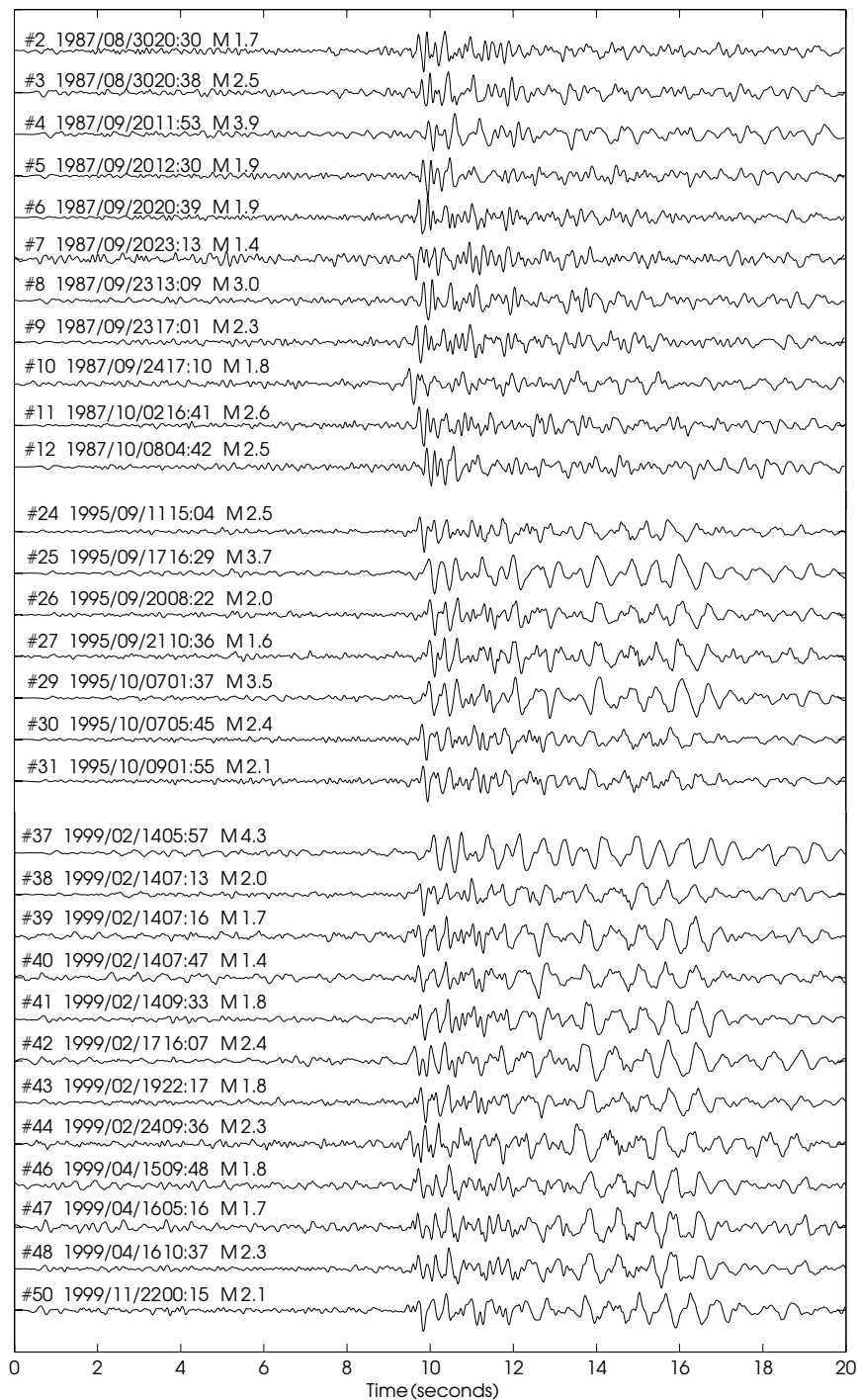
Figure 4. Seismograms (vertical component, ground velocity, zero-phase band-pass filter 1–10 Hz) of the three earthquake sequences of 1987, 1995 and 1999 recorded at station BRI. The station is situated 70 km east of the epicenters and lies close to a nodal plane of the focal mechanism, so the *Pg* arrival is the weak phase visible at about 0.5 s, and the large amplitudes at about 10 s are the *Sg* phase. Because of the emergence of the *P*-onsets at station BRI, the traces are aligned on the *P*-wave arrivals at station ROM, located at a distance of 19 km almost exactly west of the epicenters (see Fig. 6).

non-linear formulation of the earthquake location problem contains a complete description of location uncertainties. In this approach, *a priori* known errors such as measurement errors or traveltime calculation errors are explicitly incorporated in terms of probability density functions. These methods not only provide a complete description of uncertainty estimates, but can also be used with any available velocity model and method of traveltime calculation. The *P*-wave velocity adopted here was derived from a 3-D tomographic

inversion of local earthquake data with constraints from controlled source seismics (Husen *et al.* 2003). Lacking a 3-D *S*-wave velocity model, the *S*-velocities are calculated from the *P*-velocity using a V_p/V_s ratio of 1.71. The epicentral coordinates of the 1999 main shock reported in Table 1 were calculated with this method.

Based on location attempts with different combinations of stations and arrival times as well as on a comparison of location accuracies for quarry blasts in structurally similar regions, the

Table 1. Focal mechanism parameters (Murten after Pavoni 1984; Romont from Fröhlich 1989; Bulle from Baer *et al.* 2005).

Date	Time	Lat	Lon	Z	M_L	Plane1	Plane2	P	T	Event
1979/07/03	21:13	46.92	7.07	30	3.8	285/86/179	015/89/004	150/02	240/04	Murten
1987/09/20	11:53	46.768	7.217	2	3.9	007/84/002	277/88/174	322/03	232/06	Fribourg
1988/10/14	19:02	46.70	6.89	2	3.3	350/69/020	253/71/158	302/02	211/29	Romont
1995/09/17	16:29	46.788	7.216	2	3.7	175/88/003	085/87/178	310/01	040/04	Fribourg
1995/10/07	01:37	46.792	7.216	2	3.5	177/88/001	087/89/178	132/01	042/02	Fribourg
1999/02/14	05:58	46.793	7.215	2	4.3	354/88/009	264/81/178	129/05	219/08	Fribourg
2004/02/18	14:32	46.609	6.995	9	3.3	327/69/−032	070/60/−155	286/38	020/05	Bulle

Time: UTC, Z: focal depth (km), M_L: local magnitude, Plane1, Plane2: fault plane (strike/dip/rake),
P, T: compressional and extensional axis (azimuth/plunge). Plane1 is the active fault plane for all events except Murten and
Bulle, for which it is not known.

uncertainties of absolute locations of the Fribourg epicenters are judged to be on the order of 2–3 km. This uncertainty is also seen in the scatterplot obtained from the probabilistic location procedure shown in the top part of Fig. 5. Since these epicentral uncertainties are too large to resolve the small-scale geometry of possible active faults at depth, we were forced to resort to more sophisticated relative location techniques. However, before presenting these relative location results, we address the question of the focal depths of the Fribourg earthquakes.

3.2 Focal depths

The focal depths of the Fribourg earthquakes calculated routinely with a 1-D velocity model are around 15 km. A precise focal depth relying mainly on arrival times of direct waves and based on a 1-D velocity model can only be determined if the distance between the epicenter and the closest station is not larger than about 1.5 times the focal depth. In the case of the Fribourg events, the closest station is an accelerometer at a distance of 13–14 km (SLAE in Fig. 6). Unfortunately, it was not equipped with a time-signal receiver, so that only the *S-P* arrival time differences are usable for location purposes. However, the station is situated on poorly consolidated quaternary sediments, whose thickness and shear-wave velocities are not known with sufficient accuracy to be of any real use. The next closest station is ROM at a distance of 19 km. This is already at the limit of what would be desirable. In addition, station ROM is located in the Molasse Basin, where the near-surface velocity structure deviates significantly from what is assumed in the routinely used velocity model, so that, at an epicentral distance of about 19 km, the arrival times at this station are likely to introduce a systematic bias towards larger focal depths. Indeed, at least for the M_L 4.3 event of 1999, a focal depth of 15 km is not compatible with the observed macroseismic intensity field and with results from a full-waveform moment tensor inversion: both the rapid fall-off with distance of the macroseismic intensities and the waveform inversion, with a best fit at 4 km, suggest a much shallower focal depth (Deichmann *et al.* 2000). This is corroborated by the depth of 5–6 km, which results from the probabilistic location procedure using the 3-D velocity model. This value would place the hypocenter of the 1999 event in the crystalline basement. However, as shown in the bottom plot of Fig. 5, the remaining uncertainty does not preclude the possibility that the source is actually located in the overlying sediments.

In an attempt to constrain the focal depths further, we resorted to modelling the observed traveltimes with the use of the 2-D seismic ray-tracing program MODD (Gebrande 1976). Based on independent velocity information obtained from reflection and refraction surveys, detailed velocity models along selected profiles were constructed. For our study, information on shallow structures and velocity (upper 5 km) of northern Switzerland is provided by

Pfister (1990). To determine the thickness of the layers he used the correlated data of seismic reflection profiles provided by NA-GRA (Sprecher & Müller 1984), stratigraphic borehole data as well as geologic data (Naef *et al.* 1985; Laubscher 1985, 1987;
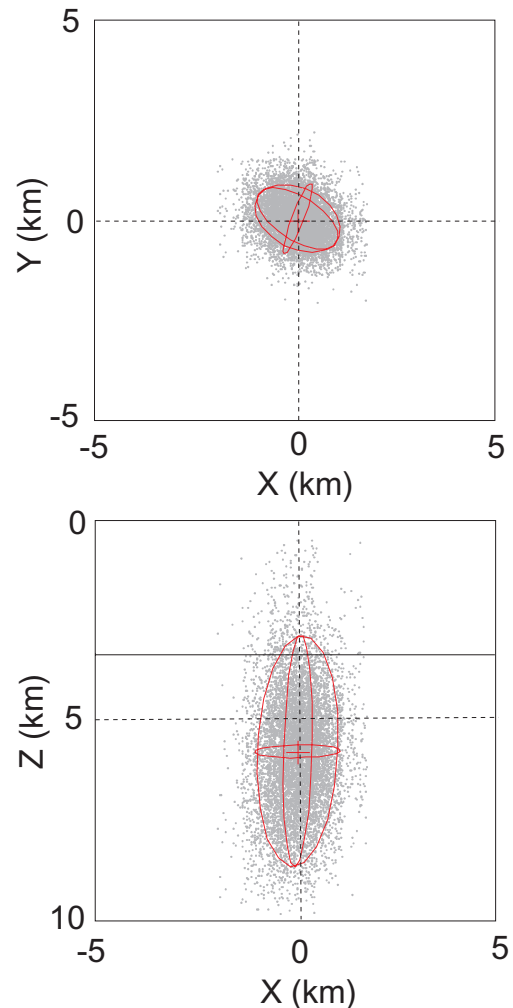
Figure 5. Epicenter map (top) and E–W cross-section (bottom) of scatterplot and 68 per cent confidence ellipsoid of the absolute location for the M_L 4.3 event of 1999/02/14 obtained from the probabilistic location procedure described in the text. The density of the scatter plot corresponds to the probability with which the true location is likey to deviate from the computed value. The continuous line in the lower plot delineates the top of the crystalline basement at about 3.5 km depth.

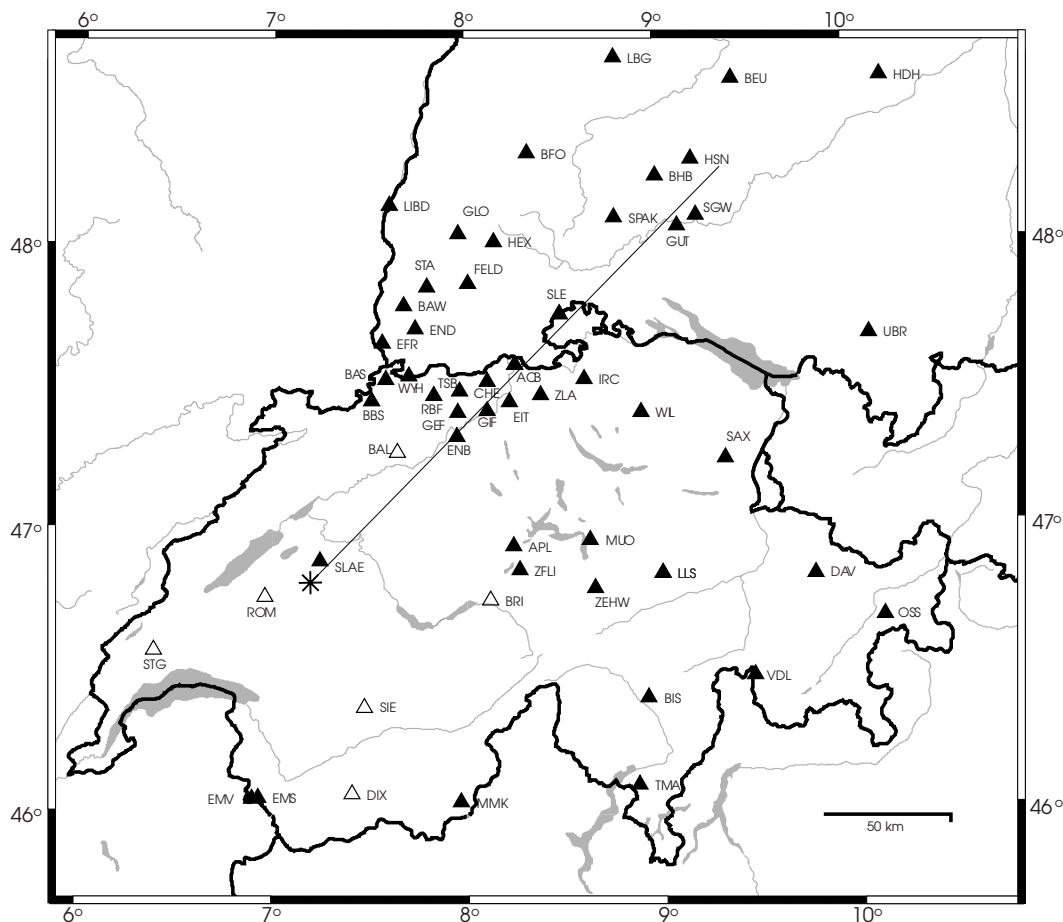**Figure 6.** Station map with the ray-trace profile shown in Fig. 7. Stations denoted by empty triangles were used in the relative location procedure.

NAGRA 1988; Matter 1987). For velocity information he used NAGRA borehole data compiled by Sierro (1989), results from sonic logs (NAGRA 1988), velocity information from seismic refraction profiles (Fromm *et al.* 1984), as well as data from *P*-velocity studies in the Molasse Basin (Lohr 1969). Crystalline velocities in the area of the Black Forest (Germany) are from Schler (1993), who inverted first arrival times of *P*- and *S*-waves of local earthquakes to model a 3-D distribution of *P*- and *S*-velocities. The Moho depth is from Waldhauser *et al.* (1998). The focal depth was varied until the theoretical arrival-time differences between the direct wave (*Pg*) and the phases reflected (*PmP*) and refracted (*Pn*) at the Moho match the observations. Since in this procedure we model only traveltime differences, errors in origin time are of no consequence.

As an example, in Fig. 7 we show the ray-tracing results and the match with the observed seismograms along a profile in NE direction from Fribourg towards the Swabian Jura (see the station map in Fig. 6). In Fig. 7, the seismograms at distances between 80 and 150 km are those of the M_L3.7 event of 1995/09/17, whereas the signals beyond 180 km are from the M_L4.3 event of 1999/02/14. Combining the signals of these two events in the same record section is justified by the close proximity of their hypocenters (shown in the next section) and was necessary, because the records at the shorter distances are clipped for the 1999 event and those at larger distances are missing for the 1995 event. The best fit between model and observations is obtained for a focal depth of about 7 km. This is in good agreement with the value 5–6 km obtained from the 3-D location procedure. The difference with respect to the 10 km reported

in Deichmann *et al.* (2000) is due to the use of more appropriate data for the Moho topography and a more detailed velocity model. We have also tried to model the traveltimes assuming the hypocenter to lie within the sedimentary cover at a depth of 3.5 km. Within the given uncertainties of onset times and model parameters, such a shallow focal depth can not be excluded on the grounds of the traveltime differences between *PmP* and *Pg*, and the calculated crossover distance of the *Pn* matches the observations if the Moho depth is assumed to be systematically shallower by 1–2 km with respect to the Moho map of Waldhauser *et al.* (1998).

Given the still remaining focal depth uncertainties and prompted by a critical review of a first version of this article, we searched the recorded seismograms for features, which, when compared to synthetic seismograms, could help to discriminate between a source in the sedimentary layers or in the crystalline basement. For the calculation of synthetic seismograms, we used the program package REFMET, that is based on the reflectivity method, originally developed by Fuchs (1968). In the course of time, the reflectivity method has been adapted and used by many researchers. The code used here is due to Ungerer (1990) and Forbriger (2003); it goes back to Fuchs & Müller (1971) and is documented extensively in Müller (1985).

Two recent articles by Kim *et al.* (2006) and by Ma & Atkinson (2006) demonstrate how depth phases, such as the *S* to PMP or the *S* to *Pn* conversion at the Earth's surface, can be used to constrain focal depths of earthquakes recorded at regional distances and how these phases can be identified in the observed signals by a comparison with synthetic seismograms. Kim *et al.* (2006) show how sensitive
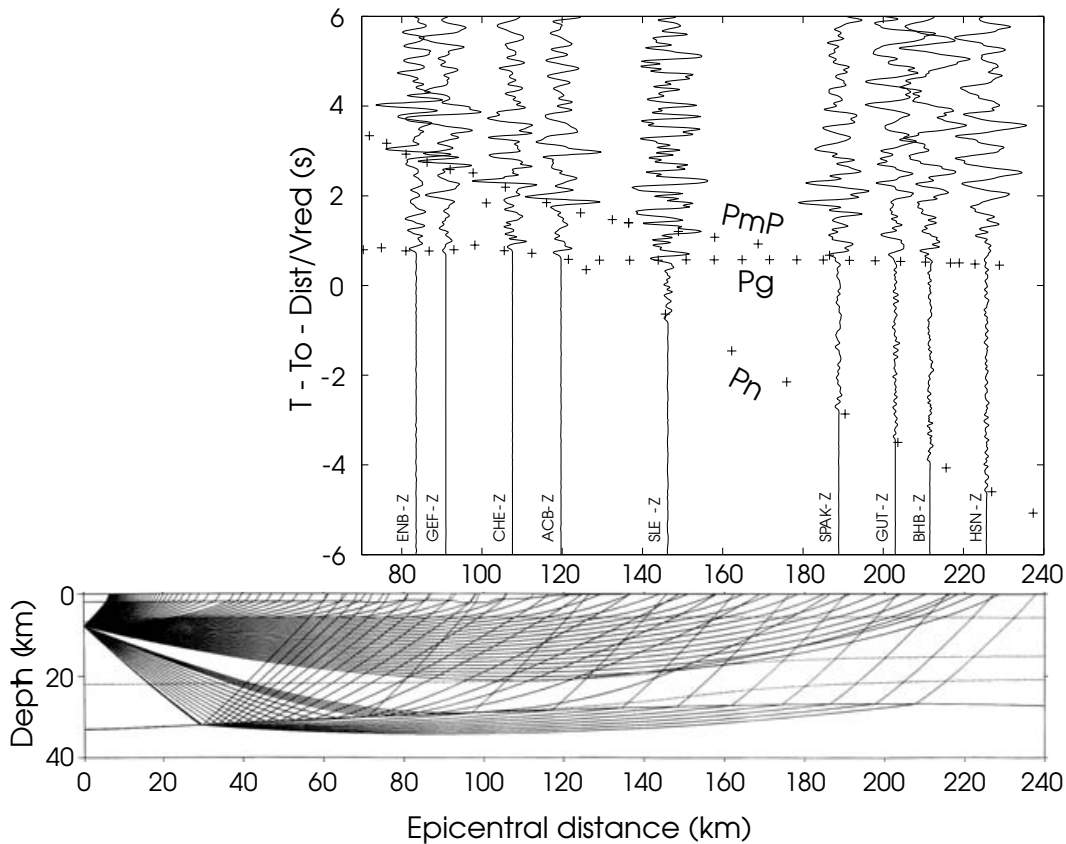
Figure 7. Seismogram record section (vertical component, zero-phase band-pass filter 0.5–12 Hz) and ray-trace diagram along a profile oriented NE from Fribourg towards the Swabian Jura. Computed traveltimes for a focal depth of 7 km are shown by crosses in the record section. The prominent arrival at distances between 80 and 150 km that follows the PMP with a constant delay of about 1.2 s is the sPMP.

to focal depth the traveltime difference between sPMP and PMP is. In the case of the Fribourg earthquakes, a particularly fine example of the sPMP phase can be seen in the record section in Fig. 7: it is the prominent arrival that follows the PMP with a constant delay of about 1.2 s at distances between 80 and 150 km. Since the Moho rises only slowly between Fribourg and these stations, the crustal structure can be approximated by a 1-D velocity model, as required by the reflectivity code. Fig. 8 shows the seismic velocities used to calculate the synthetic seismograms in Fig. 9. As a source for the synthetics we chose a vertical strike-slip fault with an orientation compatible with the known focal mechanism of the Fribourg events. As can be seen from the synthetic seismograms in Fig. 9, and as was verified by explicit traveltime calculations, the delay between sPMP and PMP at an epicentral distance of 120 km increases from 1.15 s for a focal depth of 2 km to 2.7 s for a depth of 6 km. For the chosen velocity model, the best match with the observed signal (vertical component seismogram of the $M_L 3.7$ event of 1995, recorded at station ACB) is obtained for a focal depth of 2 km. For a given focal depth, the traveltime difference between sPMP and PMP depends only on the seimic velocities between the source and the Earth's surface. Thus, for shallow earthquakes, errors in the velocity model assumed for the synthetic seismogram calculations will have a negligible effect on the results. In our case, with sediment thicknesses in the source region on the order of 3.5 km, higher seismic velocities for the sedimentary layers than those shown in Fig. 8 would not alter the conclusion that at least the source of the $M_L 3.7$ event of 1995 was not located in the crystalline basement but in the overlying sediments. In a qualitative way, this conclusion is supported also by the observation
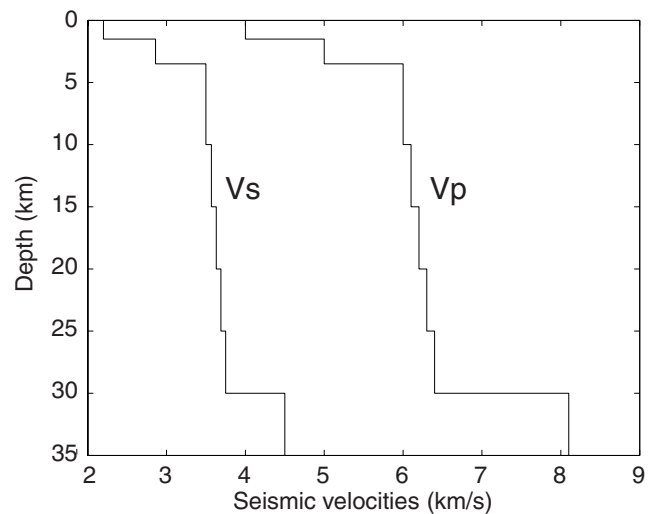
Figure 8. Velocity model used to calculate the synthetic seismograms.

that the pronounced surface waves seen in the recorded seismograms are reproduced in the synthetics only for hypocenters located at 2 and 3 km whithin the sediments, while they are practically absent for sources located in the basement (Fig. 9).

That the hypocenters of other events of the Fribourg cluster must also be located in the sedimentary cover, can be seen from the signal comparison in Fig. 11. Here we show the first 2 s of the seismograms
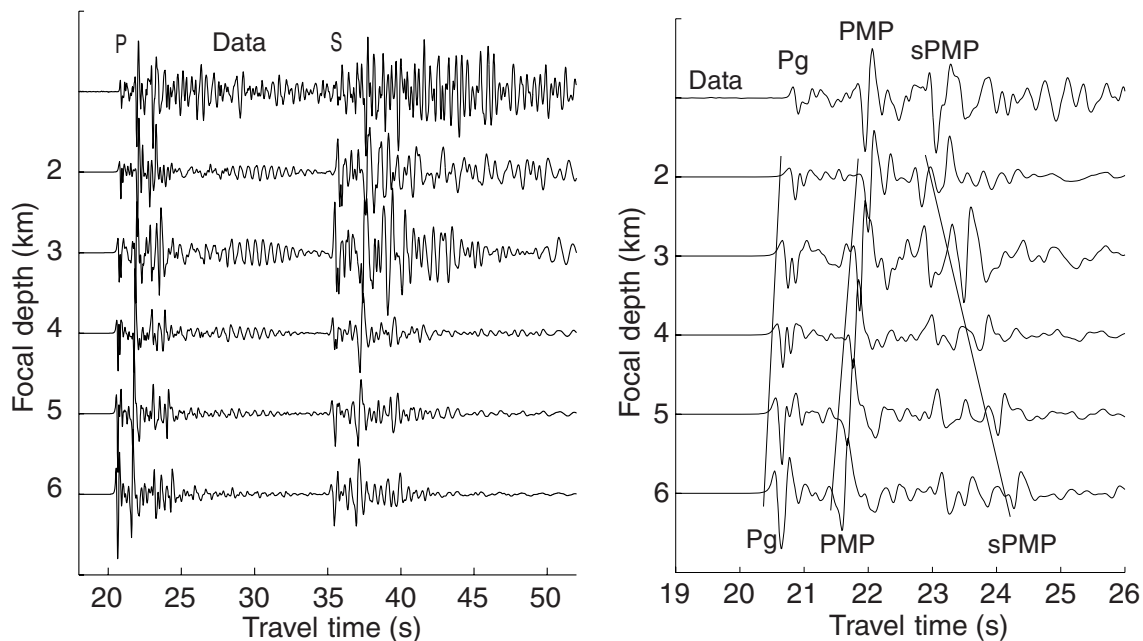
Figure 9. Top traces: vertical component seismograms of the M_L 3.7 event of 1995 recorded at station ACB (epicentral distance 120 km). Bottom traces: synthetic seismograms (high-pass filtered at 1 Hz to match the seismometer response of the observed signals) for focal depths of 2–6 km. Note the increase of the traveltime difference between sPMP and PMP with increasing depth and the good match between the observed and the synthetic seismograms for a depth of 2 km. Note also the pronounced surface waves in the observed seismogram as well as in the synthetic seismograms for sources in the sedimentary layers at depths of 2 and 3 km.

of four of the strongest events recorded in 1987, 1995 and 1999 at station CHE. The traces have been aligned on the first break of the direct wave arrival (*Pg*). The small variations in the onset times of the wave reflected at the Moho (*PmP*) indicate that focal depth differences for the hypocenters must be small. Indeed, ray-trace calculations, taking into account the differences in epicentral locations, which are presented in the next section, and allowing for the dip in the Moho, demonstrate that the focal depth differences are on the order of 200–300 m for these four events. Referring back to the discussion of the overall signal similarities shown in Fig. 4, it is evident that all the hypocenters of the Fribourg cluster are located in the sedimentary cover.

We have discussed the focal depth determination of these eathquakes in such detail, because we feel that it is an instructive example of how difficult it can be in practice to arrive at a reliable estimate of this fundamental parameter. This is particularly true for shallow earthquakes. 2-D ray-trace modelling of traveltimes of reflected and refracted phases at the Moho is a useful tool to constrain the focal depth relative to the depth of the Moho, particularly of lower crustal events. For shallow events, however, errors in crustal velocities and in Moho depth can lead to erroneous conclusions. The case of the Fribourg earthquakes is such an example. In addition, it suggests that the Moho model of Waldhauser *et al.* (1998) as well as the assumed lower-crustal velocities in NW Switzerland might need to be revised.

3.3 Cross-correlations and relative locations

The high degree of similarity of the signals shown in Fig. 4 is evidence for the close relative proximity of the hypocenters and for the similarity of the focal mechanisms. The similarity of the seismograms allows the use of cross-correlation techniques to determine relative arrival times with uncertainties that are smaller than the
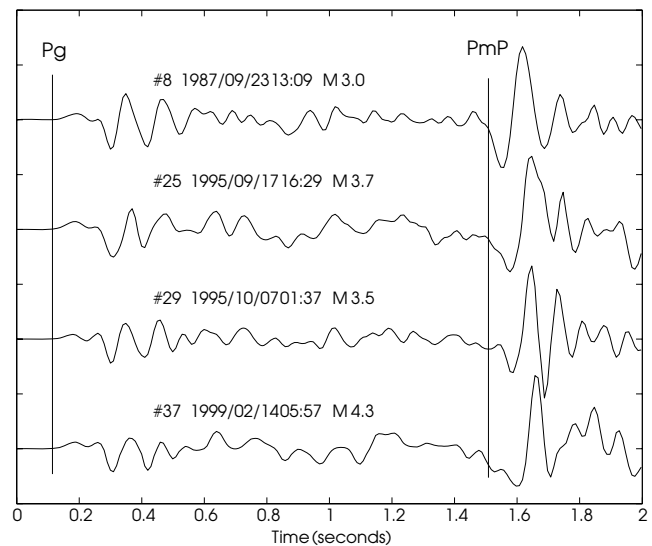
Figure 10. Seismograms of four of the strongest events recorded at station CHE, located 108 km NE of the epicenters (vertical component, ground velocity, unfiltered). Note the almost identical traveltime differences between *PmP* and *Pg* for all four events.

data sampling interval. Numerous comparable studies have shown that the relative locations of hypocenters within a particular cluster define a plane which coincides with one of the nodal planes of the fault plane solution (e.g. Deichmann & Garcia-Fernandez 1992; Augliera *et al.* 1995). Due to the common propagation paths, the location error related to incorrect velocity models is the same for all events in a particular cluster and has therefore no influence on the accuracy of the relative locations.
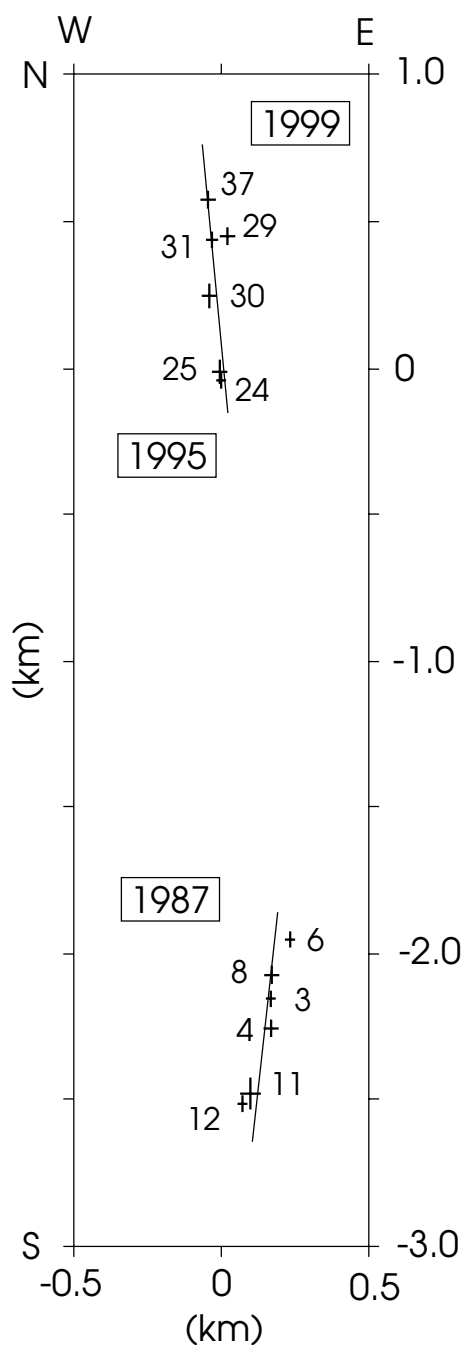
Figure 11. Relative epicenter locations based on signal cross- correlations and master event relocation. The size of the crosses is proportional to the location error (1 standard deviation). The oblique lines through the epicenter clusters delineate the strike of one of the nodal planes of the corresponding focal mechanism (see Fig. 12).

The cross-correlation procedure adopted in this study results in arrival-time differences for each event in a particular cluster relative to a chosen master event (Deichmann & Garcia-Fernandez 1992). For the calculation of the relative locations from these arrival-time differences we used an algorithm based on the method proposed by Console & DiGiovambattista (1987). The method is based on the assumption that the spatial traveltime derivatives are constant for all events. This is equivalent to assuming that the vertical and horizontal take-off angles of the rays to a particular station are the same for all

earthquakes in a given cluster. Provided the epicentral distances are much larger than the dimensions of the cluster, this approximation is valid, and then the intrinsically non-linear earthquake location problem becomes linear and trivial to solve.

Since the whole Fribourg data set comprises three different sequences and spans a large magnitude range, it was not possible to choose a single master event for all. We therefore performed the cross-correlation for the 1987 and the 1995 sequences separately, and then combined these with each other by means of the correlation of all events with a magnitude of at least 3. For all events we were able to use *P*-wave data recorded at stations ROM, SIE, BAL and BRI (see station map, Fig. 6). For some of the events we also used *S*-phases at these stations and *P*-wave data from stations STG and DIX. The azimuthal coverage given by these stations is excellent, resulting in well constrained relative epicentral locations. However, just as for the absolute focal depths, the large minimum epicentral distance did not allow the relative depths to be constrained. In the relative location calculations we therefore fixed the focal depth to the same value for all events. Since the data is not sensitive to the focal depth, fixing the relative depth of all events to a common value does not bias the determination of the horizontal coordinates.

In principle, the relative location algorithm would also allow arrival-time differences between *PmP* phases to be used and thus could add a useful constraint on the relative focal depths of the events within a single cluster. In the case of the Fribourg events, however, good-quality *PmP* arrivals are not available for a sufficient number of station and event combinations. In addition, the difference in epicentral location between the 1987 cluster and the 1995–1999 clusters is too large to be able to neglect the added effect of the dipping Moho.

The resulting relative epicentral locations for those events for which sufficient seismograms were available for cross-correlation are shown in Fig. 11. As could already be expected from the differences and similarities in signal character visible in Fig. 4, the 1987 and 1995–1999 events form two tightly grouped clusters that are clearly separated from each other by a gap of about 2 km. The two clusters align along a N–S direction, and within each cluster the distribution of epicenters is also linear over a distance of 700 to 800 m, with a roughly N–S orientation.

3.4 Focal mechanisms

We constructed focal mechanisms for the strongest shocks of each of the three sequences. Focal mechanisms of local earthquakes are very sensitive to the correct identification of the arrivals and depend on accurate estimates of the take-off angle of the rays leaving the source. In our case, the required take-off angles were taken from the ray-trace models with the hypocenters in the sedimentary cover. For this reason, all rays are either refracted at the top of the basement or at the Moho and thus the first motions appear in the stereographic plots on two concentric rings. Due to excellent azimuthal station coverage, the resulting focal mechanisms are very well constrained (Fig. 12). All of the solutions correspond to almost pure strike-slip mechanisms with more or less N–S and E–W striking nodal planes. Again, as expected from the signal similarities visible in Fig. 4, the mechanisms of the 1995 and 1999 sequences are almost identical and differ slightly from the mechanism of the 1987 sequence. These differences in the orientation of the nearly N–S striking nodal planes match also the differences in the epicenter alignments resulting from the relative locations shown in Fig. 11. It is thus evident that the
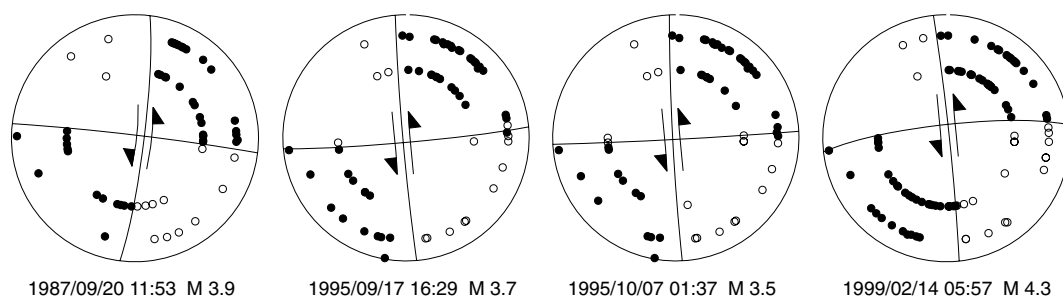
1987/09/20 11:53 M 3.9   1995/09/17 16:29 M 3.7   1995/10/07 01:37 M 3.5   1999/02/14 05:57 M 4.3

Figure 12. Fault plane solutions (lower hemisphere, equal area projections) of the four strongest Fribourg events. Filled circles represent compression (first motion up), empty circles dilation (first motion down). The active fault planes, whose strike matches the corresponding epicenter alignment shown in Fig. 10, are marked by a pair of arrows.

Fribourg earthquakes occurred as left-lateral slip on more or less N–S oriented fault planes.

4 SEISMIC REFLECTION DATA

Since 1974 several hundred kilometers of seismic reflection lines have been acquired by oil companies in the Fribourg area. The data are proprietary and most of it is unpublished. Interpretations of selected data sets have been published by Berger & Gundlach (1990) and Meier (1994). Three conceptual seismic profiles as interpreted from the data by Berger & Gundlach (1990) are shown in Fig. 13. The lines trend approximately E–W, perpendicular to the N–S striking fault planes derived from the focal mechanisms of the earthquakes in the vicinity of Fribourg. The sections A-A′, B-B′ and C-C′ show the interpretation of top Tertiary, Jurassic, Triassic and basement rocks. On the two northern profiles A-A′ and B-B′, Berger and Gundlach also see evidence for Permian sediments. According to them, the top of the basement was difficult to identify. The assumed depth of about 3400 m, however, agrees well with the depths of the crystalline basement suggested by the magnetic data (see the following section and Fig. 14). The faults visible on the interpretation extend from the Tertiary Molasse rocks down into the basement. They show compressional as well as extensional elements. Normal faulting is seen best at the base of the Triassic sediments on all interpretations as well as on the two southern profiles, B- B′ and C-C′, where Tertiary and Jurassic sediments are offset. Compressional structures are clearly visible on all sections, partly reactivating preexisting normal faults. The interpreted fault pattern shows a N–S trending graben system of approximately 50 km length with prevailing E–W extension in the South and an increasingly dominant left lateral strike-slip component in its northern part. The graben is expected to extend beneath the thrusts to the south, where E–W extension is the driving deformational force caused by thrust loading. This extension of N–S striking faults into the Prealps is consistent with observations made by Plancherel (1979). The stress state derived from recent earthquake data for this area and probabaly also prevailing during Tertiary deformation is characterized by an orientation of the greatest and least compressive stress axes that is (strike/plunge) 348/59 and 235/13 (Kastrup *et al.* 2004). Consequently, the lateral movement along N–S trending faults is and was sinistral. The interpretation by Meier (1994, reproduced in Kastrup 2002) is similar to the one presented here. According to Meier (1994), there is not enough evidence of basement faults cutting through the Mesozoic and Tertiary rocks. While he agrees that deformation in the overburden is triggered by movements along faults in the basement and that there might be younger faults that indeed cut through, he states that faults in the Mesozoic sediments, which are related to the

Tertiary deformation, have probably been deformed and dislocated from their former basement fault. Berger & Gundlach (1990) call the Molasse Basin a 'piggy back basin', which shows the crosscutting relationship between reactivated basement faults that propagate through the detachment surface and deform the allochthonous basin fill.

The identification of N–S trending fault systems east and west of the Fribourg Syncline in close vicinity to the fault system revealed by the Fribourg earthquakes (Fig. 13), is consistent in both interpretations. Due to restricted data coverage, the fault system mapped by Meier (1994) east of the Fribourg Syncline does not cover the immediate sourrounding of the Fribourg earthquakes but only the area to the north. There he maps at the base of the Tertiary two fault elements both about 9 km long. Berger & Gundlach (1990), however, conceptually connect the faults in the eastern part of the cross-sections to correlate the eastern margin of the graben over a length of 50 km.

5 MAGNETIC DATA

The map in Fig. 14 shows an average depth of the magnetic basement, derived from an interpretation of an aeromagnetic survey. The map is based on the logarithmic power spectra and the inversion of the analytical signal of the residual anomalies calibrated to borehole data (Klingelé 1986; Klingelé. & Müller 1987). The magnetic basement corresponds generally to the crystalline basement. The dominant trend, recognisable on the map, is the expected increase of the depth to basement towards the SE, that is, towards the deformation front of the Alps. However, north of Fribourg, the anomalous trend of the isobaths is consistent with a basement low such as a graben structure. This structure extends from the Molasse Basin into the Jura Mountains, where it terminates abruptly. To the south, the available magnetic data unfortunately do not allow to resolve its continuation. The main reason for the decreasing resolution is the increasing burial depth of the structure, which suggests a continuation of the depression to the South. Where resolved, the relative depth of the depression is greater than 600 m. The N–S striking faults, detected on the seismic profiles and plotted onto the map of the magnetic basement, are located in the deepest, central part of the depression. This suggests that the formation of the basement low triggered deformation in the overlying succession of sediments, forming a graben system parallel to the N–S trending basement depression.

This basement low could be related to a Permo-Carboniferous trough: based on the interpretation of seismic profiles, Meier (1994) maps SW–NE extending Permo-Carboniferous sediments in the areas NE of Lake of Neuchâtel and west of the non-interpretable
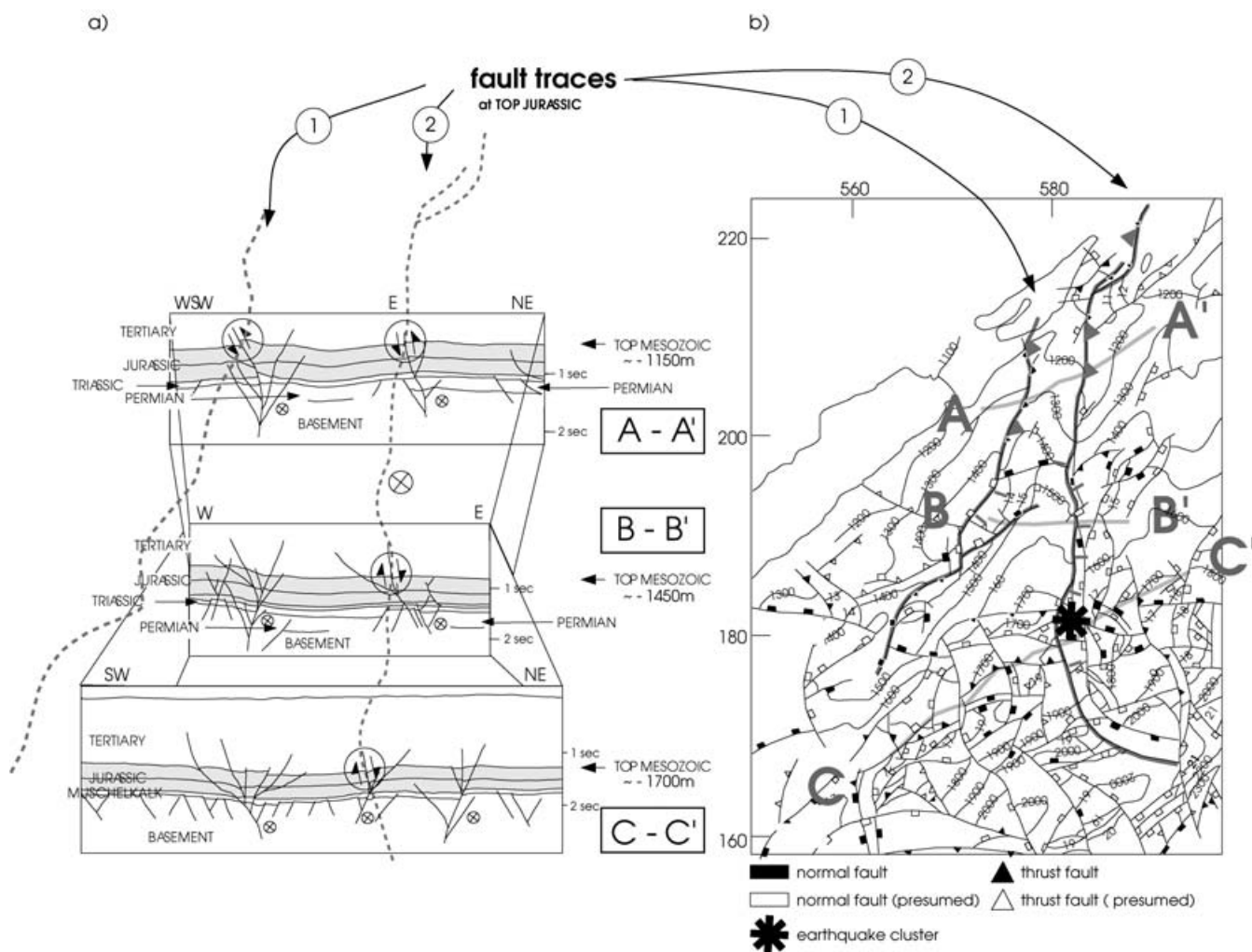
Figure 13. Structural model based on three E–W striking seismic profiles, cross-cutting the postulated fault zone around Fribourg (Berger & Gundlach 1990). The seismic sections reveal compressional structures along N–S striking faults propagating from the basement up into the Molasse sediments. The fault traces at the top Jurassic, derived from these sections as well as from additional seismic data, are shown on the right. Note the close proximity of the Fribourg hypocenters to one of the faults. Also, the strike of this fault is in agreement with the strike of the active fault planes.

zone around Fribourg. Both areas correspond to regions where the depth of the crystalline basement was found to deviate from the normal trend (Fig. 14). As the Permo-Carboniferous sediments are deposited in troughs in the basement they could be the reason for deeper depths of the crystalline basement found in these areas. Thus the region around Fribourg, where the depth of the crystalline basement could not be determined, could also be the location of a N–S striking Permo-Carboniferous trough. In fact, Berger & Gundlach (1990) found evidence for Permian sediments on the two northern profiles (Fig. 13).

6 DISCUSSION AND CONCLUSIONS

6.1 Tectonic implications

This integrated study of the western Swiss Molasse Basin in the area of Fribourg shows that there is strong evidence for large-scale N–S striking faults at depth in the southern continuation of the eastern margin of the Rhine Graben. The detailed analysis of the earthquakes studied here demonstrates that they have been generated on one or two N–S striking fault segments, situated in the sedimentary cover.

The interpretation of reflection seismic data east of Fribourg also shows extensional and strike-slip faults that involve the basement. Moreover, an additional smaller earthquake sequence near Romont, which occurred in 1988 at a depth of only 1–2 km, indicates that the Mesozoic and Tertiary sediments are still undergoing deformation today (Fröhlich 1989) and the magnitude 3.8 Murten earthquake of 1979 (Pavoni 1984) documents similar deformation in the lower crust at depths as large as 30 km (Fig. 15 and Table 1).

According to Ziegler (1990), two sets of faults, one striking NNE–SSW, the other ESE–WNW, cut through the basement in *S*-Germany and N-Switzerland in Pre-Permian times. We postulate, based on their comparable character, that the Fribourg basement faults are also of that age. They might even represent faults bordering a N–S striking Permo-Carboniferous trough, which is assumed to continue to the NE and SW of Lake of Neuchâtel. Over geological times, the detected N–S striking faults experienced at least two phases of Tertiary reactivation (Berger 1994): first as normal faults during early stages of rifting of the Rhine-Bresse-System and later during loading of the basin floor by continuous thrusting and by the latest left-lateral shear dominated rifting stage of the Rhine Graben. A correlation of the basement faults and those faults in the Mesozoic/Tertiary
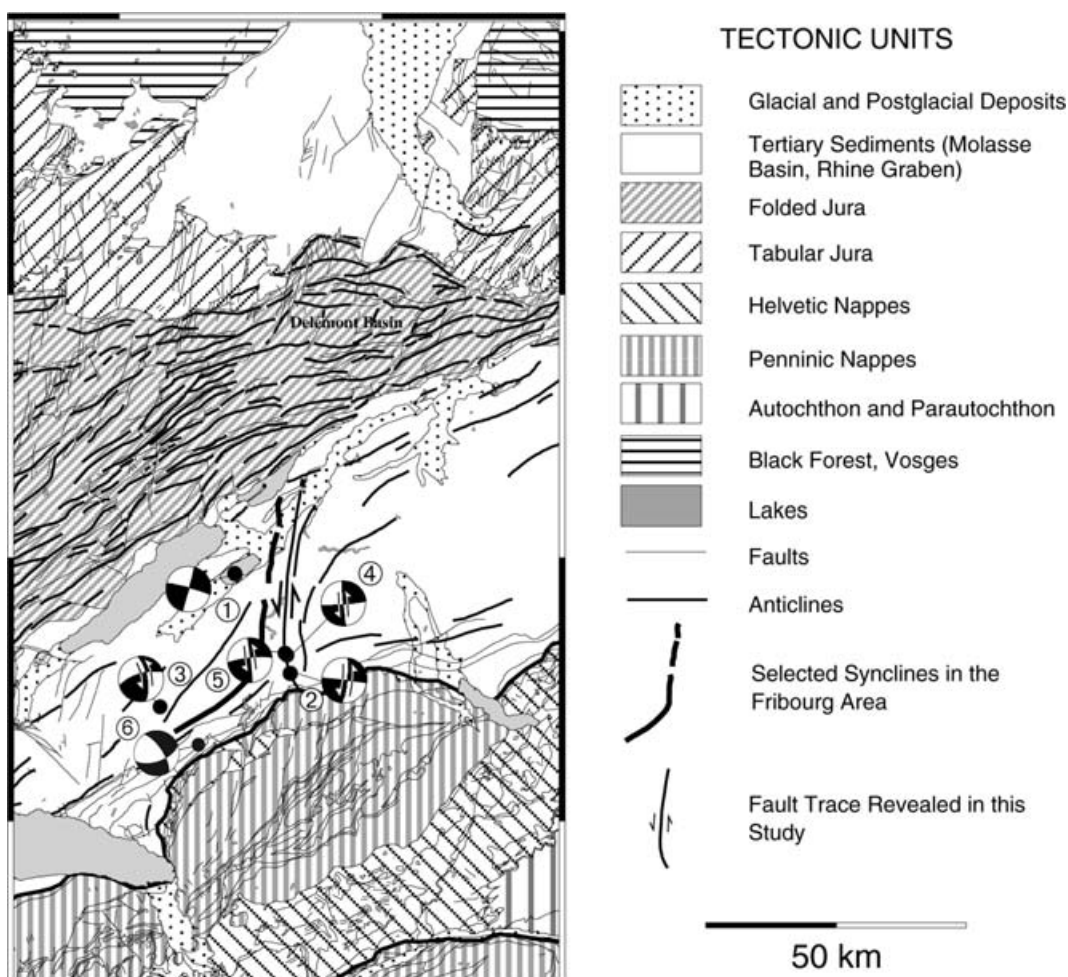
Figure 14. Map of the isobaths of the magnetic basement, which is assumed to correspond to the crystalline basement (Klingelé. & Müller 1987). It shows a depression north of Fribourg that could correspond to a N–S striking graben structure. The data in the shaded area could not be interpreted, due to the increasing depth of the basement. The dark grey lines in the shaded area are the fault traces at the top Jurassic as derived from seismic interpretation. They suggest a graben bounded by N–S striking faults.

cover can be concluded, based on the similarity in deformational style, orientation and location of the faults defined by both the seismic reflection data and the earthquake epicenter alignment. The involvement of the uppermost basement during the Miocene deformation argues against the distant-push hypothesis postulated by Laubscher (1961), which would require a smooth surface (e.g. Gorin *et al.* 1993; Pfiffner 1997). The N–S striking synclines and anticlines around Fribourg can be explained as the surface expression of the Miocene deformation of predominantly Molasse sediments overlaying the active sinistral strike-slip fault systems in the basement. A continuation of the faults to the north cannot be demonstrated in the Molasse rocks. However, tectonic maps, satellite imagery data and their interpretation as well as topographic maps show several major exposed left lateral strike-slip faults in the northern continuation of the interpreted Fribourg feature that cut through the Jura Mountains and extend into the southern part of the Rhine Graben (Berger & Gundlach 1990). Thus, for example, the detached Delémont Basin, shown on the map in Fig. 15 is bounded by two NNE–SSW striking left lateral strike-slip faults with some associated E–W shortening. Even though there might not be one long discrete fault extending from the Rhine Graben into the Molasse Basin or—as suggested by Plancherel (1979)—even further into the Prealps south of the Molasse Basin, there is evidence for faults in the Jura Mountains as well as in the Molasse Basin that follow the same basement trend and that connect the southern end of the exposed Rhine Graben with the Jura and Fribourg faults. The N–S striking epicenter alignment, its coincidence with the strike of the active fault plane and the agree-

ment with structural interpretations of geomorphological, seismic reflection and magnetic data constitute convincing evidence for the existence of an active fault in the region of Fribourg.

6.2 Hazard implications

To assess what implications an active fault might have for the seismic hazard of the Fribourg region, we must examine the historical seismicity and estimate magnitudes of potential earthquakes that could be associated with a reactivation of this fault.

Of the events analyzed in this study, the earthquake of February 14th, 1999 with $M_L = 4.3$ and $M_w = 4.0$ (Deichmann *et al.* 2000) was the strongest. Its epicentral intensity, I_o, reached V. The newly revised Earthquake Catalog of Switzerland, ECOS, (Fäh *et al.* 2003) lists 7 additional events with intensity $I_o \geq$ V located within a distance of 10 km from the epicenter of this earthquake (Table 2). The two events of 1880 listed in Table 2 with $I_o =$ VI occurred within two days of each other. In this case it is difficult to associate the available historical macroseismic information unequivocally to one or the other event, so that the epicentral intensity of the first event is doubtful. Considering that the catalog is probably not complete for $I <$ VI before 1820 (Fäh *et al.* 2003), it is clear that the area around Fribourg is a seismically active region and that the recent activity is not exceptional.

Though the active fault planes of the main events of the 1987 sequence and of the two sequences of 1995 and 1999 do not have

Figure 15. Seismotectonic map for the western part of the Molasse Basin with the inferred N–S striking fault close to the Fribourg clusters. Focal mechanisms: 1 - Murten 1979, 2 - Fribourg 1987, 3 - Romont 1988, 4 - Fribourg 1995, 5 - Fribourg 1999, 6 - Bulle 2004.

Table 2. Events with $I_o \geq V$ in the vicinity of Fribourg listed in the Earthquake Catalog of Switzerland, ECOS.

Date	Lat	Lon	X/Y	I_o	Event
1617/07/05	46.80	7.17	579/183	V	Fribourg
1662/04/06	46.80	7.17	579/183	V	Fribourg
1873/04/10	46.80	7.16	579/183	V	Fribourg
1880/09/19	46.82	7.18	580/185	VI	Fribourg
1880/09/21	46.82	7.18	580/185	VI	Fribourg
1904/03/28	46.77	7.24	585/180	V	Rechthalten
1926/12/15	46.75	7.17	579/178	V	Praroman
1999/02/14	46.79	7.21	583/181	V	Fribourg

X/Y Swiss National Coordinates (km), I_o Epicentral Intensity (EMS98).

the exact same orientation (Fig. 11), they could be patches of a single fault that is slightly curved and is at least 3.5 km long. If one accepts that the epicenters, which are also aligned in a N–S direction and which extend beyond the segment defined by the relative locations in Fig. 11, occurred on the same fault, then the length of this fault amounts to 20–30 km. Unfortunately we do not know the focal mechanisms of these additional events, but the orientation and extent of the geomorphological features and the geophysical evidence lend

support to the existence of a fault at depth that is several tens of km long.

Fig. 16 shows the range of moment magnitudes, M_w, that are expected for a given fault rupture length based on an empirical compilation by Wells & Coppersmith (1994) and on two theoretical models. The continuous bold line in Fig. 16 corresponds to the regression of Wells & Coppersmith (1994), while the two thin continuous lines give an approximate indication of the magnitude spread of the data (± 0.5 mag units) from which the regression was calculated. The theoretical relations were calculated for a circular and a rectangular fault model, assuming values of static stress drop, $\Delta\sigma = 1$, 10 and 100 bar (0.1, 1 and 10 MPa). These relations were derived from the definition of seismic moment $M_0 = \mu A \bar{s}$ (with μ the shear modulus, A the rupture area, $\bar{s}$ the average slip), the definition of moment magnitude $M_w = 2/3 \log M_0 - 6$ (for M_0 in N m, Hanks & Kanamori 1979) and the definition of static stress drop $\Delta\sigma = C\mu\bar{s}/W$ (with C a coefficient that depends on the mode of faulting and on the aspect ratio of the fault and with W the width of the fault in m). For a circular fault of radius R the expression for the stress drop becomes $\Delta\sigma = (7/16)\pi\mu\bar{s}/R$ (with $W = 2R$ and $C = 2.75$ this expression is equivalent to the previous one). Combining these equations and defining an aspect ratio $a = L/W$ between fault length and width for the rectangular fault and setting $L = 2R$
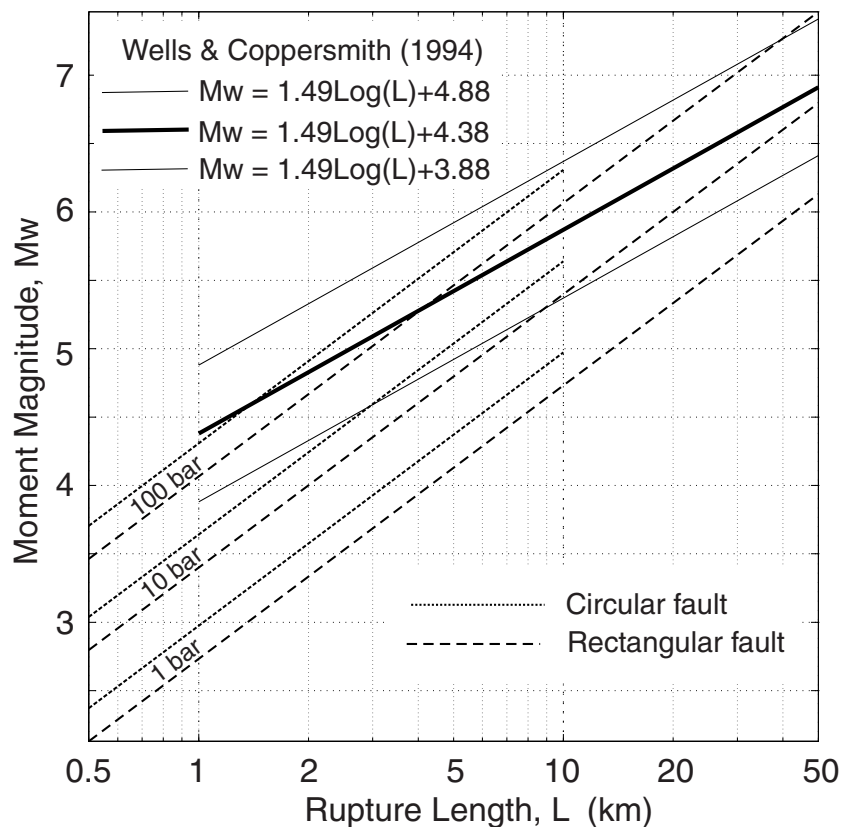
Figure 16. Moment magnitude, M_w, as a funtion of rupture length, L, based on the empirical regression of Wells & Coppersmith (1994) and on theoretical calculations for a circular and rectangular fault for three different static stress drops. Different line lengths reflect the range of the available data or of the applicability of the model.

for the circular fault, we obtain expressions for M_w as a function of $\Delta\sigma$ and the rupture length L for the rectangular and circular faults:

$$M_w = 2\log L + \frac{2}{3}\log\Delta\sigma - \frac{4}{3}\log a - \frac{2}{3}\log C - 6$$

$$M_w = 2\log L + \frac{2}{3}\log\Delta\sigma - 6.36.$$

For the case of the rectangular fault, we assume an aspect ratio of 2:1; this value corresponds to the ratio of rupture length to rupture width for $M_w = 6$, if one combines the regressions of Wells & Coppersmith (1994) for M_w with respect to L and W (their Figs 14 and 15). Moreover, we set the coefficient $C = 2$, which corresponds to the mean between the theoretical values $C = 1.3$ for an infinitely long fault and $C = 2.7$ for a circular fault. Since we lack any information to constrain the stress drop, the range of possible magnitudes of events associated with a given rupture length is large. Nevertheless, it is clear from Fig. 16 that had the fault segment, which was active between 1987 and 1999, ruptured in a single event with a stress drop in the range of 10 bar, it would probably have attained a magnitude between 4.5 and 5. In an epicentral area that is as densely populated as the city of Fribourg, some damage is to be expected even from such a moderate earthquake, particularly when its source is shallow. A perfect example of such an event is the M_L 5 Epagny earthquake of 1996/07/15, which occurred at a depth of 3 km on the Vuache Fault and which caused shaking intensities of VII–VIII (e.g. Baer *et al.* 1997; Thouvenot *et al.* 1998). If we accept that the fault is actually 20–30 km long and that it could rupture in a single event, then this earthquake can easily reach a magnitude around 6. According to a

more recent empirical study by Mai & Beroza (2000), even a 10 km long fault can generate earthquakes with M_w in the range between 5.8 and 6.2. An earthquake with a magnitude in this range is likely to cause severe damage to the city of Fribourg and surrounding towns.

is contribution number 1499 of the Institute of Geophysics, ETH Zurich.

REFERENCES

Ahorner, L., Murawski, H. & Schneider, G., 1972. Seismotektonische Traverse von der Nordsee bis zum Apennin, *Geol. Rundschau,* **61**(3), 915–942.

Augliera, P., Cattaneo, M. & Eva, C., 1995. Seismic multiplets analysis and its implication in seismotectonics. In: Focal mechanism and seismotectonics, *Tectonophysics,* **248**(3–4), 219–234.

Baer, M. *et al.*, 1997. Earthquakes in Switzerland and surrounding regions during 1996, *Eclogae geol. Helv.,* **90**(3), 557–567.

Berger, Z., 1994. *Satellite hydrocarbon exploration, interpretation and integration techniques*, Springer, 219 p.

Berger, Z. & Gundlach, T., 1990. The Contribution of Satellite Interpretation to Exploration in west Germany and Switzerland. BEB, Task Force Exploration strategy, Report No.3.

Burkhard, M., 1990. Aspects of the large-scale Miocene deformation in the most external part of the Swiss Alps (Subalpine Molasse to Jura fold belt), *Eclogae geol. Helv.,* **83**(3), 559–583.

Console, R. & DiGiovambattista, R., 1987. Local earthquake relative location by digital records, *Phys. Earth planet Inter.,* **47**, 43–49.

Deichmann, N. & Garcia-Fernandez, M., 1992. Rupture geometry from high-precision relative hypocentre location of microearthquake cluster, *Geophys. J. Int.,* **110**, 501–517.

Deichmann, N. *et al.*, 2000. Earthquakes in Switzerland and surrounding regions during 1999, *Eclogae Geol. Helv.,* **93**(3), 395–406.

Deichmann, N. *et al.*, 2004. Earthquakes in Switzerland and surrounding regions during 2003, *Eclogae Geol. Helv. - Swiss J. Geosciences,* **97**(3), 447–458.

Deichmann, N. *et al.*, 2006. Earthquakes in Switzerland and surrounding regions during 2005, *Eclogae Geol. Helv. - Swiss J. Geosciences,* **99**(3), 443–452.

Fäh, D. *et al.*, 2003. Earthquake catalog of Switzerland (ECOS) and the related macroseismic database, *Eclogae Geol. Helv. - Swiss J. Geosciences,* **96**(2), 219–236.

Forbriger, T., 2003. Notizen zur Berechnung synthetischer Seismogramme mit der Reflektivitätsmethode. Report, BFO Schiltach, Germany.

Fröhlich, A., 1989. Seismotektonik der Westschweiz unter Beruecksichtigung der Bebenserie von Freiburg (1987), Romont (1988) und Boltigen (1989). Diplomarbeit, Institut für Geophysik, ETH-Zürich.

Fromm, G., Driessen, L. & Lehner, I., 1984. Geophysikalisches Untersuchngsprogramm der Nordschweiz: Refraktionsseismische Messungen 84. NAGRA Technical Report, NTB 84–43, Nagra, Baden, Switzerland.

Fuchs, K., 1968. The reflection of spherical waves from transition zones with arbitrary depth-dependent elastic moduli and densitiy. Special issue, *J. Phys. Earth,* **16**, 27–41.

Fuchs, K. & Müller, G., 1971. Computation of synthetic seismograms with the reflectivity method and comparison with observations, *J. R. Astr. Soc.,* **23**, 417–433.

Gebrande, H., 1976. A seismic ray-tracing method for two-dimensional inhomogeneous media, in *Explosion seismology in central Europe*, pp. 162–167, eds Giese P., Prodehl, C. & Stein, A., Springer.

Gorin, G.E., Signer, C. & Amberger, G., 1993. Structural configuration of the western Swiss Molasse Basin as defined by reflection seismic data, *Eclogae geol. Helv.,* **86**, 693–716.

Hanks, T.H. & Kanamori, H., 1979. A moment magnitude scale, *J. geophys. Res.,* **84**(B5), 2348–2350.

Husen, S., Kissling, E., Deichmann, N., Wiemer, S., Giardini, D. & Baer, M., 2003: Probabilistic earthquake location in complex three-dimensional velocity models: Application to Switzerland, *J. geophys. Res.,* **108**(B2), 2077–2096.

Illies, J.H., 1974. Taphrogenesis and Plate Tectonics, in *Approaches to Taphrogenesis, dynamic models for taphrogenesis*, pp. 433–460, eds Illies, J.H. & Fuchs, K.

Kastrup, U., 2002. Seismotectonics and Stress Field Variations in Switzerland, *PhD thesis*, ETH Zrich, Switzerland.

Kastrup, U., Zoback, M.L., Deichmann, N., Evans, K. & Giardini, D., 2004. Stress field variations in the Swiss Alps and the northern Alpine foreland, *J. geophys. Res.,* **109**(B1), doi:10.1029/2003JB002550B01402.

Kim, W.-Y., Dineva, S., Ma, S. & Eaton, D., 2006. The 4 August 2004, Lake Ontario Earthquake, *Seism. Res. Lett.,* **77**(1), 65–73.

Klingelé, E., 1986. Les levés aéromagnétiques de la Suisse. Geodätisch-geophysikalische Arbeiten in der Schweiz., Band 37.

Klingelé, E. & Müller, St., 1987. La cartographie du soubassement magnetique du Bassin Molassique et du Jura Suisse, *Eclogae Geol. Helv.,* **80**(1), 17–36.

Kopp, J., 1946. Zur Tektonik der westschweizer Molasse, *Eclogae geol. Helv.,* **39**(2).

Laubscher, H.P., 1961. Die Fernschubhypothese der Jurafaltung, *Eclogae geol. Helv.,* **52**, 221–282.

Laubscher, H.P., 1985. The eastern Jura: Relations between thin-skinned and basement tectonics, local and regional, NAGRA Technical Report, NTB 85–53, Baden, Switzerland.

Laubscher, H.P., 1987. Die tektonische Entwicklung der Nordschweiz, *Eclogae geol. Helv.,* **80**(2), 287–303.

Lee, W.H.K. & Lahr, J.C., 1972. HYPO-71 a computer program for determining hypocenter, magnitude and first motion pattern for local earthquakes, Open-File Rep., U.S. Geological Survey.

Lohr, J., 1969. Die seismischen Geschwindigkeiten der jüngeren Molasse im ostschweizerischen und deutschen Alpenvorland, *Geophys. Prospect.,* **17**, 111–125.

Lomax, A. & Curtis, A., 2001. Fast, probabilistic earthquake location in 3D models using Oct-Tree Importance sampling. Geophysical Research Abstracts, 3.

Lomax, A., Virieux, J., Volant P. &Thierry-Berge, C., 2000. Probabilistic earthquake location in 3D and layered models, in *Advances in Seismic Event Location*, eds Thurber C.H. & Rabinowitz N., Kluwer Academic Publishers.

Ma, S. & Atkinson, G.M., 2006. Focal depths for small to moderate earthquakes ($m_N \leq 2.8$) in western Quebec, southern Ontario, and northern New York, *Bull. seism. Soc. Am.,* **96**(2), 609–623, doi: 10.1785/0120040192.

Mai, P.M. & Beroza, G.C., 2000. Source scaling properties from finite-fault-rupture models, *Bull. seism. Soc. Am.,* **90**, (3), 604–615.

Matter, A., 1987. Faciesanalyse und Ablagerungsmilieu des Permokarbons im nordschweizer Trog, *Eclogae geol. Helv.,* **80**(2), 345–367.

Meier, B.P., 1994. Untere Süsswassermolasse des westlichen Mittellandes: Regionale Interpretation bestehender Seismik und petrophysikalische Interpretation von Fremdbohrungen, NAGRA Internal Report, NIB 94–28, Baden, Switzerland.

Müller, G., 1985. The reflectivity method: a tutorial, *J. Geophys.,* **58**, 153–174.

Naef, H., Diebold, P. & Schlanke, S., 1985. Sedimentation und Tektonik im Tertiär der Nordschweiz, NAGRA Technical Report, NTB 85–14, Baden, Switzerland.

NAGRA, Sedimentstudie Zwischenbericht, 1988. Möglichkeiten zur Endlagerung langlebiger radioaktiver Abfälle in den Sedimenten der Schweiz. NAGRA Technical Report, NTB 88–25, Baden, Switzerland.

Pavoni, N., 1977. Erdbeben im Gebiet der Schweiz, *Eclogae Geol. Helv.,* **70**(2), 351–370.

Pavoni, N., 1984. Seismotektonik Nordschweiz, NAGRA Technical Report, NTB 84–45, Baden, Switzerland.

Pfiffner, O.A., 1997. Molasse Basin tectonics and its relation to the Jura Mountains, in Deep Structure of the Alps, results of NRP20, Birkhuser, Basel, 71–72.

Pfister, M., 1990. Gemeinsame Auswertung von Erdbeben-, Refraktions-und Reflexionsdaten in der Nordschweiz, Diploma thesis, Institute of Geophysics, ETH-Zürich, Switzerland.

Plancherel, R., 1979. Aspects de la déformation en grand dans les Préalpes médianes plastiques entre Rhône et Aar. Implications cinématiques et dynamiques, *Eclogae geol. Helv.,* **72**(1), 145–214.

Plancherel, R., 1996. Tektonische Karte Blatt Fribourg (1185), Geologischer Atlas der Schweiz, 1:25000.

Plenefisch, T. & Bonjer, K.-P., 1997. The stress field in the Rhine Graben area inferred from earthquake focal mechanisms and estimation of frictional parameters, *Tectonophysics,* **275,** 71–97.

Schler, T., 1993. P- and S-Wellentomographie der Erdkruste des Südschwarzwaldes unter Verwendung lokalseismischer Laufzeitresiduen, *Diploma Thesis*, Institute of Geophysics, University of Kalsruhe, Germany.

Sierro, N., 1989. Regionale Struktur der Erdkruste in der Nordschweiz, *PhD thesis*, ETH Zürich, Switzerland.

Sprecher, C. & Müller, W.H., 1984. Geophysikalische Untersuchungsprogramm der Nordschweiz: Refraktionsseismik 82, NAGRA Technical Report, NTB 84–15, Baden, Switzerland.

Thouvenot, F. *et al.*, 1998. The Ml-5.3 Epagny (French Alps) earthquake of 15 July 1996: a long awaited event on the Vuache fault, *Geophys. J. Int.,* **135,** 876–892.

Ungerer, J., 1990. Berechnung von Nahfeldseismogrammen mit der Reflektivitätsmethode. *Diploma Thesis*, Institute of Geophysics, University of Stuttgart, Germany.

Waldhauser, F., Kissling, E., Ansorge, J. & Müller, S., 1998. Three dimensional interface modelling with two-dimensional seismic data; the Alpine crust-mantle boundary, *Geophys. J. Int.,* **135**(1), 264–278.

Wells, D.L. & Coppersmith, K.J., 1994. New empirical relations among magnitude, rupture length, rupture width, rupture area and surface displacement, *Bull. seism. Soc. Am.,* **84**(4), 974–1002.

Ziegler, P., 1990. Geological Atlas of Western and Central Europe. The Hague: Shell International Petroleum Maatschappij.